Solid-State Batteries Hot Paper

How to cite: *Angew. Chem. Int. Ed.* **2021**, *60*, 6718–6723
International Edition: doi.org/10.1002/anie.202015238
German Edition: doi.org/10.1002/ange.202015238

# Lithium-Metal Anode Instability of the Superionic Halide Solid Electrolytes and the Implications for Solid-State Batteries

*Luise M. Riegger, Roman Schlem, Joachim Sann, Wolfgang G. Zeier,* and Jürgen Janek**

***Abstract:*** *Owing to high ionic conductivity and good oxidation stability, halide-based solid electrolytes regain interest for application in solid-state batteries. While stability at the cathode interface seems to be given, the stability against the lithium metal anode has not been explored yet. Herein, the formation of a reaction layer between $Li_3InCl_6$ ($Li_3YCl_6$) and lithium is studied by sputter deposition of lithium metal and subsequent in situ X-ray photoelectron spectroscopy as well as by impedance spectroscopy. The interface is thermodynamically unstable and results in a continuously growing interphase resistance. Additionally, the interface between $Li_3InCl_6$ and $Li_6PS_5Cl$ is characterized by impedance spectroscopy to discern whether a combined use as cathode electrolyte and separator electrolyte, respectively, might enable long-term stable and low impedance operation. In fact, oxidation stable halide-based lithium superionic conductors cannot be used against Li, but may be promising candidates as cathode electrolytes.*

## Introduction

Solid state batteries (SSB) are currently regarded as a possible alternative to conventional lithium ion batteries (LIB) with liquid electrolyte (LE) due to the projected higher energy densities when using a lithium metal anode (LMA).[1–3] When solidifying a battery, the solid electrolyte (SE) replaces the LE and hence requires a high ionic conductivity to achieve reasonable power densities. In addition, stability in contact with cathode active materials (CAM) is needed to prevent detrimental side reactions.[4,5] Currently, most inorganic SSBs employ lithium thiophosphates such as $Li_6PS_5X$ (X = Cl, Br, I) or Argyrodite-type SEs, $Li_3PS_4$ and $Li_{10}GeP_2S_{12}$, all of which are good ionic conductors, but which have severe drawbacks at the cathode due to their inherent instability at high potentials.[2,6]

In order to find SEs that are oxidation stable at high potentials, halides have recently been reconsidered as suitable candidates.[7] In 2018, Asano et al.[8] reevaluated halide SEs with the general composition $Li_3MX_6$ ($M^{3+}$, X = Cl, Br, I), of which mostly $Li_3InCl_6$ and $Li_3YCl_6$ have gained a lot of attention. This group of compounds exhibits a broad range of possible compositions such as for example, $Li_3InCl_6$, $Li_3YCl_6$, $Li_3YBr_6$, $Li_3ErCl_6$ and $Li_3ErI_6$,[8–14] which all show promising ionic conductivities, especially after ball-milling synthesis,[13] and high stability against oxidation that is required for the application in high-voltage SSBs.[11] First cell studies show good stability of the halide SEs in contact with CAMs such as $LiCoO_2$ and $LiNi_{0.8}Co_{0.1}Mn_{0.1}O_2$, and side reactions with the CAMs were not reported.[8–11,15] This is in accordance with theoretical predictions that suggest high oxidation stability of the halide anions.[7,14] According to theoretical predictions, the electrochemical stability windows (ESW) of $Li_3InCl_6$ and $Li_3YCl_6$ are 2.38–4.26 V and 0.62–4.02 vs. $Li^+/Li$, respectively,[14] showing that these electrolytes can be used in contact with most CAMs but that the anode interface may be unstable. Due to the expected instability against the LMA, a lithium thiophosphate separator electrolyte is mostly used, and the halide SEs are primarily used as cathode electrolyte.[8–11] Interestingly, no experimental studies on the interface stability of halide SEs against the LMA have been reported. Figure 1 shows a schematic SSB setup with the halide SE at the LMA, as well as when it is used as the cathode electrolyte only. In addition to the unexplored

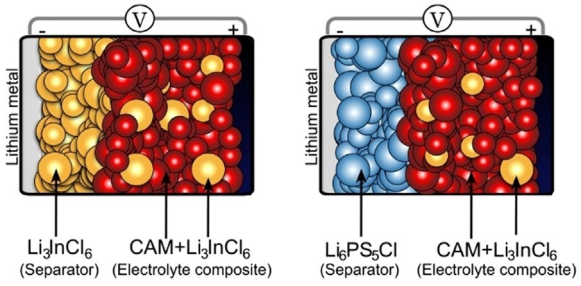


***Figure 1.*** Schematic SSB cell arrangements using $Li_3InCl_6$, a) as both separator electrolyte and cathode electrolyte with the cathode active material (CAM), b) as cathode electrolyte combined with a lithium thiophosphate separator electrolyte towards the lithium metal anode.

[*] L. M. Riegger, Dr. J. Sann, Prof. J. Janek
Institute of Physical Chemistry, Justus-Liebig-University Gießen
Heinrich-Buff-Ring 17, 35392 Giessen (Germany)
and
Center for Materials Research (LaMa), Justus-Liebig-University Gießen
Heinrich-Buff-Ring 17, 35392 Gießen (Germany)
E-mail: juergen.janek@phys.chemie.uni-giessen.de
R. Schlem, Prof. W. G. Zeier
Institute for Inorganic and Analytical Chemistry, University of Münster
Corrensstr. 30, 48149 Münster (Germany)
E-mail: wzeier@uni-münster.de
Supporting information and the ORCID identification number(s) for the author(s) of this article can be found under: https://doi.org/10.1002/anie.202015238.

reactions at the LMA interface, the interface impedance for lithium ion transfer between a lithium thiophosphate separator electrolyte and a halide-based cathode electrolyte has yet not been considered.[16]

To monitor the stability of the halide SEs $Li_3InCl_6$ and $Li_3YCl_6$ against lithium metal, we deposited lithium metal on a SE pellet and performed in situ X-ray photoelectron spectroscopy to analyze the reaction products in detail. Impedance measurements were performed to assess solid electrolyte interphase (SEI) formation between the halide SEs in contact with the LMA, and to quantify the impedance of the interface between the lithium metal halides and the lithium thiophosphate $Li_6PS_5Cl$.

In earlier work, our group investigated decomposition reactions and reaction layers that form when various thiophosphate based electrolytes such as $Li_{10}GeP_2S_{12}$, $Li_3PS_4$ or $Li_6PS_5X$ (X = Cl, Br, I) are exposed to lithium metal, using in situ X-ray photoelectron spectroscopy.[17–20] While all lithium thiophosphates are inherently unstable against lithium metal, the transport properties of the growing interphase decide whether kinetical stability is achieved: (1) If the reaction products form an mixed ion/electron conducting interphase (MCI), then a continuous reaction is expected that will ultimately lead to a short circuit of the SSB over time.[17,21] Mixed conducting interphases are typically observed in SEs that contain metal cations $M^{4+}$ (e.g. M = Ge, Ti), which are then reduced to $M^0$ after contact with lithium forming an electrically conductive reaction layer.[17,18] (2) If the decomposition products are primarily ion-conducting and show negligible electronic conductivity, growth of a stable SEI can occur. As long as the SEI growth is self-limiting and does not add a too high interphase impedance the SE may still be used, like in the case of $Li_3PS_4$ and $Li_6PS_5Cl$.[3,5,20,22]

## Results and Discussion

Figure 2 shows X-ray photoelectron spectra of $Li_3InCl_6$ during deposition, with the In-3d lines, the In-MNN Auger lines as well as the Li-1s lines for pristine $Li_3InCl_6$ after two different lithium deposition times. A pure indium metal reference was used to obtain the shape of the metal In-$3d_{5/2}$ line as well as the position of the characteristic In-MNN line, see Figure S1. In addition, $InCl_3$ was measured as reference to obtain the binding energies of an In-Cl environment. When monitoring the In-3d spectrum, an immediate change in the oxidation state was seen upon lithium deposition. The pristine sample exhibits one line at 446.1 eV, which can be assigned to $Li_3InCl_6$. After ten minutes of lithium deposition two more lines caused by $In_2O_3$ (444.8 eV) and metallic indium (443.7 eV) were found in addition to the original $Li_3InCl_6$. As thermodynamics predicts, $In^{3+}$ is reduced by lithium to form $In^0$. The occurring $In_2O_3$ signal is probably caused by an immediate reaction of the indium metal with oxygen either from a decontamination layer at the surface or with residual oxygen within the chamber. However, the $In_2O_3$ signal increases after a waiting step in the measurement chamber so the influence of residual oxygen seems to be the stronger influence. After an hour of lithium metal deposition (approx. 15 nm), the ongoing decomposition becomes even more apparent. Now the In-3d line of $Li_3InCl_6$ is significantly decreased indicating an ongoing interphase growth that buries the SE. It must be mentioned that $Li_3InCl_6$ and $InCl_3$ exhibit the same binding energy (see Supporting Information Figure S3) and it is not possible to distinguish how much of $Li_3InCl_6$ has potentially reacted to reduced indium chloride species such as $InCl_2$ and InCl.

The formation of metallic indium is also seen in the In-MNN Auger spectrum. At 1081.7 eV a characteristic line is found in $Li_3InCl_6$. Ten minutes of lithium deposition causes

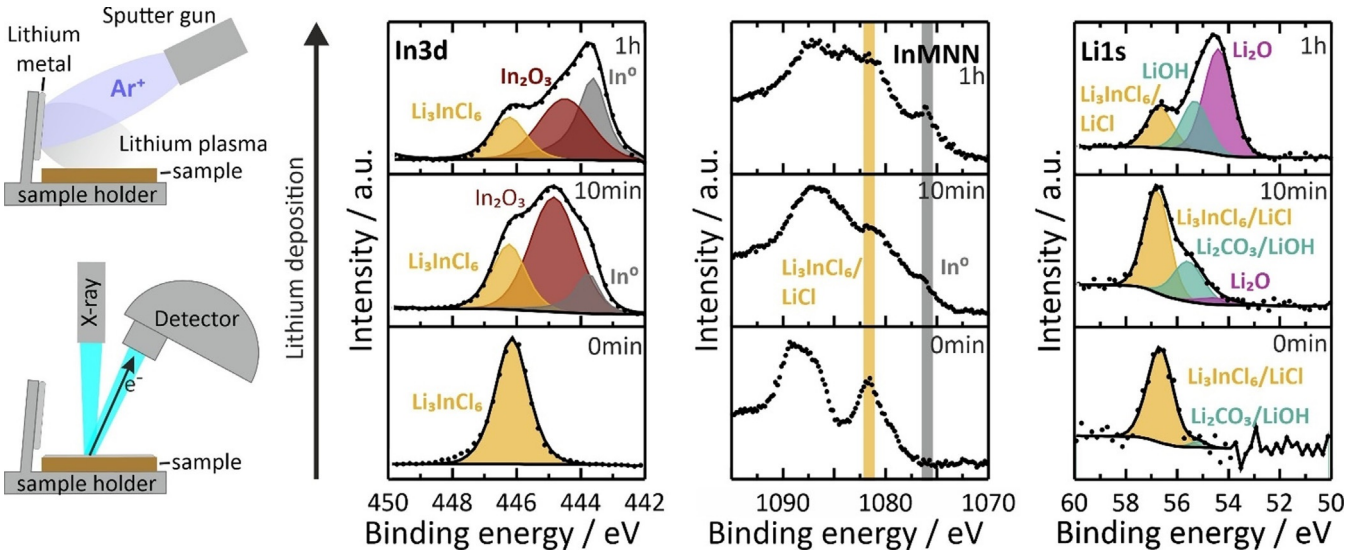


***Figure 2.*** a) Schematic illustration of lithium metal deposition on SE with an argon sputter gun and subsequent X-ray photoelectron spectroscopy. X-ray photoelectron In-3d and Li-1 s (b,d) and Auger In-MNN (c) spectra during/after lithium deposition on $Li_3InCl_6$. $Li_3InCl_6$ decomposes in contact with lithium metal to metallic indium, which readily reacts with any remaining oxygen in the UHV chamber to $In_2O_3$. The intensity of lines representing pristine $Li_3InCl_6$ decrease with time indicating coverage of the SE by the growing interphase.

  

a reduction of this $Li_3InCl_6$ signal and a second characteristic peak starts to evolve at 1076.0 eV that is characteristic of In metal (see Supporting Information Figure S1). The In metal signal is even more distinct after an hour of lithium deposition indicating that a significant fraction of the indium has become metallic.

Like in the indium spectra, the decomposition of $Li_3InCl_6$ is seen in the Li-1 s spectrum as well. The Li-1s spectrum shows $Li_3InCl_6$ with a binding energy of 56.7 eV and an additional line at 55.2 eV, which can be assigned to surface contaminations such $Li_2CO_3$ or LiOH. Within ten minutes of lithium deposition, the $Li_3InCl_6$ signal (56.8 eV) is reduced and superimposed by $Li_2CO_3$ and LiOH on the pellet surface. Similar to the In signal, the binding energy of $Li_3InCl_6$ and LiCl is the same, and no distinction can be made in the Li-1s spectrum (see Figure S3). While carbonates can be detected, after ten minutes of lithium deposition, $Li_2O$ is detected at a binding energy of 54.3 eV (Figure S2). After an hour of deposition, the $Li_2O$ signal (54.4 eV) dominates the Li-1s spectrum and the $Li_3InCl_6$/LiCl (56.7 eV) and LiOH (55.3 eV) signals are significantly decreased. The decrease of LiOH can be rationalized either due to a reaction with lithium metal to form $Li_2O$ or by superposition of the $Li_2O$ signal. While lithium metal is constantly deposited on top of the sample, no metallic lithium was detected indicating its quick reaction and ongoing decomposition of the $Li_3InCl_6$ and possible further reactions of Li with the interphase (vide infra).

In addition to $Li_3InCl_6$, the spectra of $Li_3YCl_6$ recorded in situ during lithium deposition can be found in the Figures S4 and S5. Similar to $Li_3InCl_6$, yttrium is reduced upon contact between $Li_3YCl_6$ and lithium as shown in Figure S4. $Y^{3+}$ is reduced to $Y^0$ within ten minutes of lithium deposition and $Y^0$ then reacts further with decontaminations of the antechamber or neighboring species forming $Y_2O_3$ or $Y_2(CO_3)_3$, which results in a broadened XPS signal. Similar to $Li_3InCl_6$, signals of the reduced yttrium components become stronger with time indicating an advancing reaction front. The Li-1s spectra of the $Li_3YCl_6$ show the same behavior as in $Li_3InCl_6$ in which the $Li_3YCl_6$/LiCl signals decrease with deposition time and are being superposed by newly formed $Li_2CO_3$, LiOH and $Li_2O$.

Considering the measured spectra during decomposition with Li metal, we propose the following idealized net reaction:

$$Li_3MCl_6 + 3Li \rightarrow 6LiCl + M^0 \qquad (M = In,Y) \tag{1}$$

Of course, intermediate reduced species such as $InCl_2$ and InCl may form as indicated in the Cl-2p spectrum (Supporting Information, Figure S2) by shifting towards the binding energy of $InCl_3$. However, these species cannot be distinguished in the measured spectra. From the thermodynamic perspective, the ongoing reaction will ultimately end at a fully reduced metal species. Clearly, the in situ deposition experiments prove that the halide SEs are unstable against lithium metal, showing a continuously growing reaction layer.

To study SEI growth, time resolved impedance spectroscopy was performed on $Li_3InCl_6$ symmetric cells with lithium metal electrodes. Figure 3 a shows the impedance spectrum of $Li_3InCl_6$ with blocking electrodes to obtain the typical capacitance of bulk $Li_3InCl_6$, which was found to be 20 pF together with an ionic conductivity of 0.5 mS cm$^{-1}$. Figure 3 c then shows the collected impedance spectra (15 min intervals at the beginning, then 30 min and later 1 hour intervals). The collected time-resolved spectra were fitted with an equivalent circuit consisting of three parallel $RQ$ elements in series ($R$: resistance, $Q$: constant phase element, CPE). Figure 3 b shows an exemplary fit of one impedance spectrum and the capacitances evaluated for the three processes. Bulk conduction within $Li_3InCl_6$ is observed at high frequencies with a capacitance of 84.3 pF (pellet thickness is a quarter of the pellet with the blocking electrodes). A low frequency process is visible that we attribute to the Li | SE (or better Li/SEI) interface as a much higher capacitance of 3.1 μF is observed due to the planar electrodes. In addition, a third process is visible in the intermediate frequency range (0.7 MHz to 4 kHz). The capacitance of this process with 8.4 nF indicates a grain boundary process, likely indicative of the growing interphase. This process, while described via one constant phase element/resistor element, shows low α values of down to 0.65.[23] It is therefore highly likely that multiple underlying processes with quite close relaxation times are occurring, indicating a rather distributed microstructural and compositional nature of the forming interphase.

When extracting the resistances of the different processes (see Figure 3 d), the bulk contribution does not vary significantly with time. The resistance that is assigned to the interphase (cyan) is continuously growing with time, together with the interface resistance (blue) towards Li, and a high overall interfacial resistance of 854 Ω has already formed after one hour. Based on the classification by Wenzel et al.[24] the ongoing growth of the interphase together with the growing resistance is indicative of an SEI in which the ionic conductivity of the interphase is lower than the conductivity of the bulk electrolyte. If Equation (1) applies, the SEI is formed from a composite of indium metal in LiCl.[25] The volume fraction of indium from the decomposition reaction compared to LiCl is relatively small (1:8), and the SEI resistance may be dominated by LiCl. Interestingly enough, the decomposition behavior leading to a mixed-conducting interphase is observed in $Li_3YCl_6$ as shown in the Supporting Information, Figure S6. At this point, the discrepancy between the transport behavior of $Li_3InCl_6$ and $Li_3YCl_6$ may be explained by the fact that indium is prone to alloying with Li already at room temperature.[26] This LiIn alloy formation would form a metal electrode dispersed within LiCl as an electrolyte, which shows the behavior of a SEI development in the impedance measurement.[25] In any case, both $Li_3InCl_6$ and $Li_3YCl_6$ are clearly exhibiting fast decomposition at the LMA and cannot be used as separator electrolyte materials in SSBs.

$Li_3InCl_6$ and $Li_3YCl_6$ have been tested in SSBs as cathode electrolyte components, whereas thiophosphates are often also used as separator electrolyte material.[8–11] In order to employ halide-based SEs as cathode electrolytes in combination with thiophosphate SEs, the transfer resistance at their interface needs to be sufficiently small. In order to study this interfacial resistance a symmetric cell setup was used

  

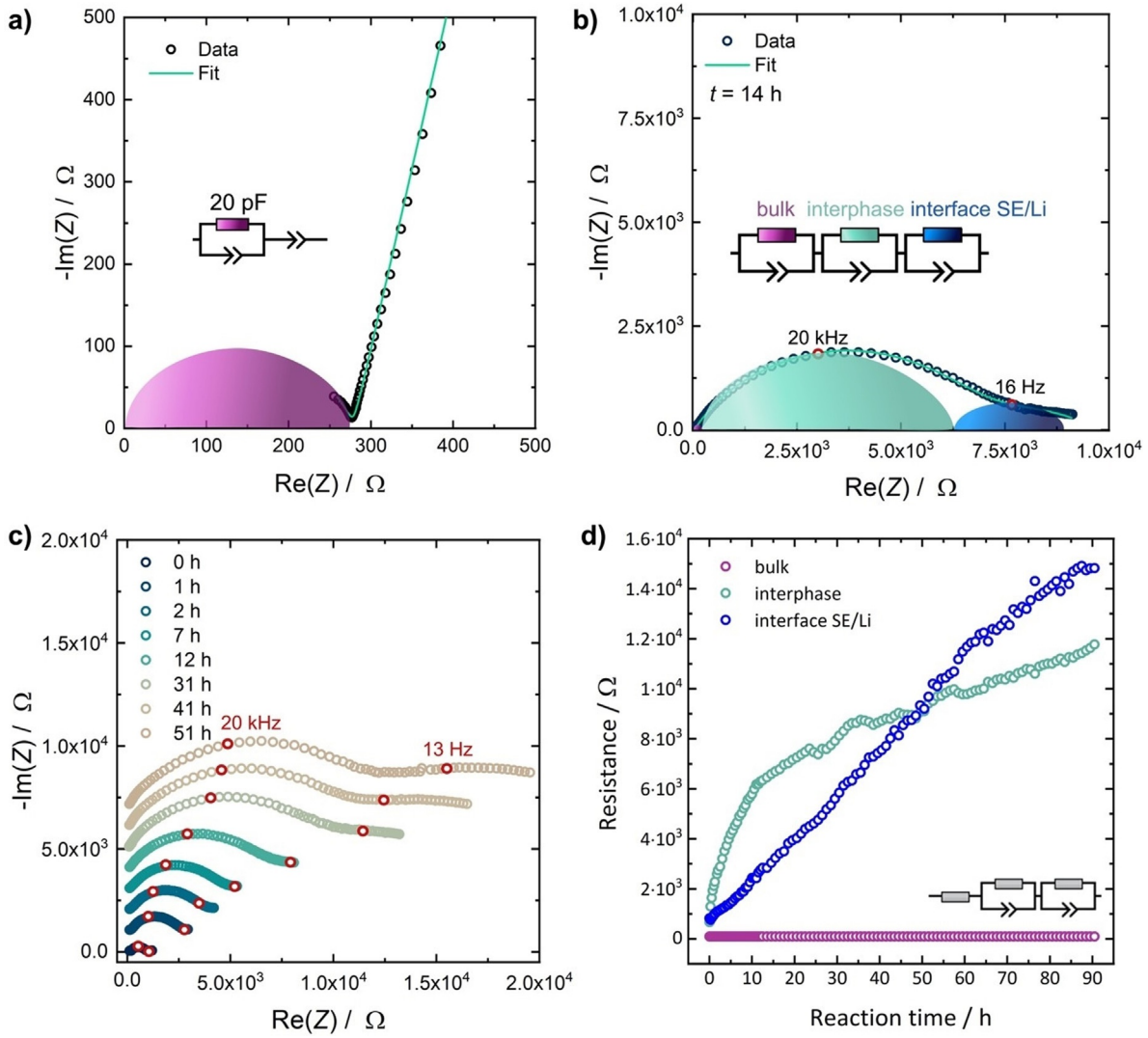


***Figure 3.*** a) Impedance spectra of $Li_3InCl_6$ using blocking electrodes. b) Representative fit of an impedance spectrum of a symmetric cell Li/$Li_3InCl_6$/Li after 14 hours, showing the bulk transport process in $Li_3InCl_6$ (shown in purple), the interface Li/SEI (blue) and the growing resistance of the interphase (cyan). c) Temporal evolution of the impedance response of a symmetric Li | $Li_3InCl_6$ | Li cell, stacked without rescaling and shifted by 1 kΩ for each spectrum. d) Temporal evolution of the resistances of the different processes.

consisting of a $Li_3InCl_6$ pellet sandwiched between a layer of $Li_6PS_5Cl$ with Li electrodes on each side. At room temperature, only one process is visible in the impedance spectrum (see Figure 4a). To resolve the respective ionic transfer process, the impedance was measured at low temperatures down to 173 K. Figure 4a shows a representative Nyquist Plot at 193 K, as well as a schematic of the cell setup and the used equivalent circuit as insets. At these temperatures, a single semi-circle was observed for the bulk contribution, which is indicative for virtually similar fast conduction in both electrolytes and a combined capacitance of 51.8 pF, indicative of a bulk process. A second process is found that corresponds to the $Li_6PS_5Cl$ | $Li_3InCl_6$ interphase with a capacitance of 0.4 μF. The high capacitance rules out that these are grain boundary resistances, as these are expected to have capacitances in the nF range. The deconvolution of both processes provides the respective resistances, which are shown in Figure 4b. A slightly higher activation barrier for the ion transfer between $Li_6PS_5Cl$ and $Li_3InCl_6$ is found compared to bulk transport. Overall the $Li_6PS_5Cl$ | $Li_3InCl_6$ charge transfer resistance is roughly one order of magnitude smaller than the bulk contribution and is 59 Ω cm$^2$ compared to 589 Ω cm$^2$ for the bulk process at 193 K, thus it is negligible at room temperature. This small resistance for Li ion charge transfer at the hetero-contact $Li_6PS_5Cl$ | $Li_3InCl_6$ supports the general finding that the interface resistance two inorganic SEs is small, once good contact is achieved.[16]

## Conclusion

In conclusion, this communication reports firstly on the instability of $Li_3InCl_6$ and $Li_3YCl_6$ at the LMA. Decomposition by reduction is found via in situ X-ray spectroscopy that leads to a fast-growing interphase, which is detrimental for the overall cell resistance. This rules out the use of lithium metal

  

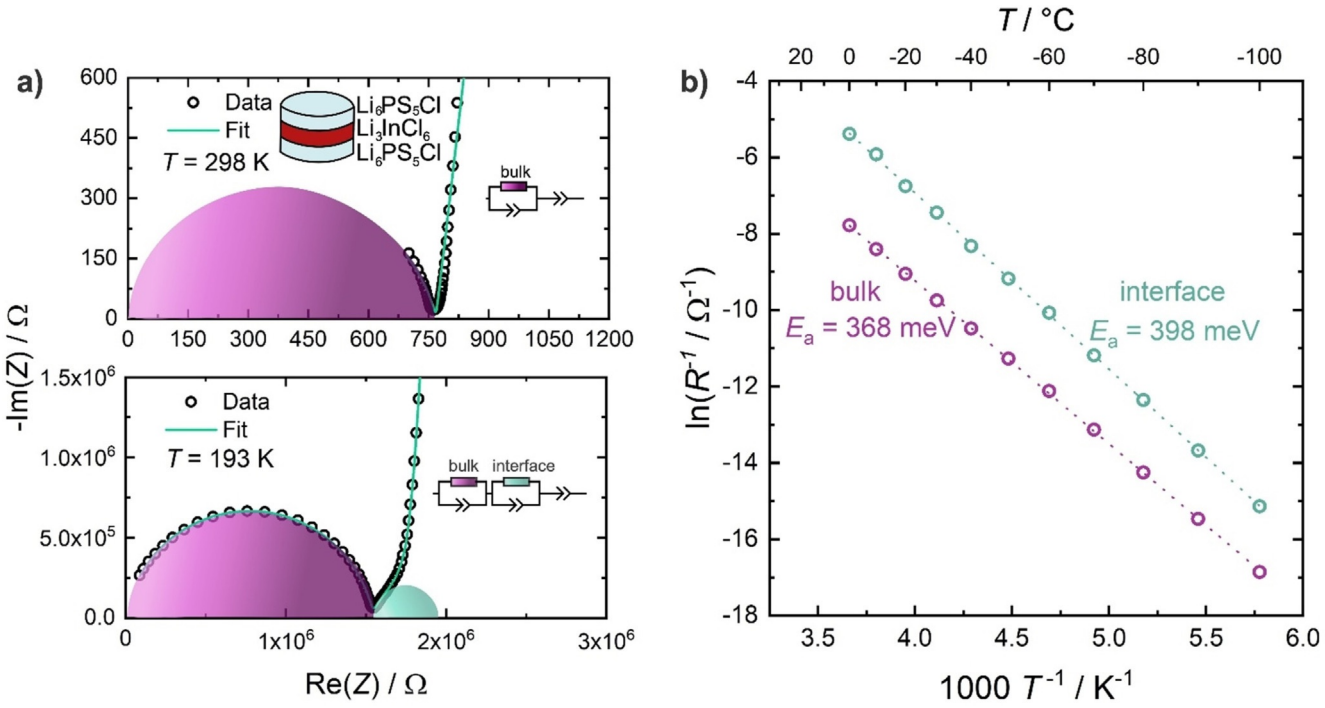


***Figure 4.*** a) Representative impedance of the symmetric $Li_6PS_5Cl\,|\,Li_3InCl_6\,|\,Li_6PS_5Cl$ sandwich cell at room temperature and 193 K. While both processes cannot be deconvoluted at room temperature and are described well with a single bulk process (40 pF) at lower temperatures a clear assignment can be made corresponding to a bulk (51.8 pF) and an interface contribution (0.4 µF). b) Arrhenius behavior of the two processes in the bulk and at the $Li_6PS_5Cl\,|\,Li_3InCl_6$ interface.

halides as separator electrolyte materials in SSBs with LMA. Secondly, a relatively low interface impedance is measured at the (unoptimized) $Li_6PS_5Cl\,|\,Li_3InCl_6$ interface. Thus, the combination of stable SEI-forming $Li_6PS_5Cl$ together with $Li_3InCl_6$ as cathode electrolyte, or the use of the halide SE as a stable coating of an CAM, may be a suitable solution in practice.

## Acknowledgements

The research was supported by the Federal Ministry of Education and Research (BMBF) within the project FEST-BATT under grant numbers 03XP0117A and 03XP0176D. We greatly appreciate helpful discussions with S. Burkhardt. Open access funding enabled and organized by Projekt DEAL.

## Conflict of interest

The authors declare no conflict of interest.

**Keywords:** electrochemical energy storage · lithium metal anode · solid electrolyte interphase · solid-state batteries · x-ray photoelectron spectroscopy

[1] a) J. Janek, W. G. Zeier, *Nat. Energy* **2016**, *1*, 1167; b) J. Betz, G. Bieker, P. Meister, T. Placke, M. Winter, R. Schmuch, *Adv. Energy Mater.* **2019**, *9*, 1803170.
[2] Y.-G. Lee, S. Fujiki, C. Jung, N. Suzuki, N. Yashiro, R. Omoda, D.-S. Ko, T. Shiratsuchi, T. Sugimoto, S. Ryu, et al., *Nat. Energy* **2020**, *5*, 299.
[3] S. Randau, D. A. Weber, O. Kötz, R. Koerver, P. Braun, A. Weber, E. Ivers-Tiffée, T. Adermann, J. Kulisch, W. G. Zeier, et al., *Nat. Energy* **2020**, *5*, 259.
[4] a) S. P. Culver, R. Koerver, T. Krauskopf, W. G. Zeier, *Chem. Mater.* **2018**, *30*, 4179; b) S. P. Culver, R. Koerver, W. G. Zeier, J. Janek, *Adv. Energy Mater.* **2019**, *9*, 1900626; c) W. D. Richards, L. J. Miara, Y. Wang, J. C. Kim, G. Ceder, *Chem. Mater.* **2016**, *28*, 266.
[5] R. Koerver, F. Walther, I. Aygün, J. Sann, C. Dietrich, W. G. Zeier, J. Janek, *J. Mater. Chem. A* **2017**, *5*, 22750.
[6] a) F. Walther, R. Koerver, T. Fuchs, S. Ohno, J. Sann, M. Rohnke, W. G. Zeier, J. Janek, *Chem. Mater.* **2019**, *31*, 3745; b) J. Auvergniot, A. Cassel, J.-B. Ledeuil, V. Viallet, V. Seznec, R. Dedryvère, *Chem. Mater.* **2017**, *29*, 3883; c) W. Zhang, D. A. Weber, H. Weigand, T. Arlt, I. Manke, D. Schröder, R. Koerver, T. Leichtweiss, P. Hartmann, W. G. Zeier et al., *ACS Appl. Mater. Interfaces* **2017**, *9*, 17835; d) R. Koerver, I. Aygün, T. Leichtweiß, C. Dietrich, W. Zhang, J. O. Binder, P. Hartmann, W. G. Zeier, J. Janek, *Chem. Mater.* **2017**, *29*, 5574.
[7] S. Muy, J. Voss, R. Schlem, R. Koerver, S. J. Sedlmaier, F. Maglia, P. Lamp, W. G. Zeier, Y. Shao-Horn, *iScience* **2019**, *16*, 270.
[8] T. Asano, A. Sakai, S. Ouchi, M. Sakaida, A. Miyazaki, S. Hasegawa, *Adv. Mater.* **2018**, *30*, 1803075.
[9] X. Li, J. Liang, N. Chen, J. Luo, K. R. Adair, C. Wang, M. N. Banis, T.-K. Sham, L. Zhang, S. Zhao, et al., *Angew. Chem. Int. Ed.* **2019**, *58*, 16427 – 16432; *Angew. Chem.* **2019**, *131*, 16579 – 16584.

  

[10] X. Li, J. Liang, J. Luo, M. Norouzi Banis, C. Wang, W. Li, S. Deng, C. Yu, F. Zhao, Y. Hu, et al., *Energy Environ. Sci.* **2019**, *12*, 2665.
[11] K.-H. Park, K. Kaup, A. Assoud, Q. Zhang, X. Wu, L. F. Nazar, *ACS Energy Lett.* **2020**, *5*, 533.
[12] a) X. Li, J. Liang, X. Yang, K. R. Adair, C. Wang, F. Zhao, X. Sun, *Energy Environ. Sci.* **2020**, *13*, 1429; b) R. Schlem, T. Bernges, C. Li, M. A. Kraft, N. Minafra, W. G. Zeier, *ACS Appl. Energy Mater.* **2020**, *3*, 3684.
[13] R. Schlem, S. Muy, N. Prinz, A. Banik, Y. Shao-Horn, M. Zobel, W. G. Zeier, *Adv. Energy Mater.* **2020**, *10*, 1903719.
[14] S. Wang, Q. Bai, A. M. Nolan, Y. Liu, S. Gong, Q. Sun, Y. Mo, *Angew. Chem. Int. Ed.* **2019**, *58*, 8039; *Angew. Chem.* **2019**, *131*, 8123.
[15] a) J. Liang, X. Li, S. Wang, K. R. Adair, W. Li, Y. Zhao, C. Wang, Y. Hu, L. Zhang, S. Zhao, et al., *J. Am. Chem. Soc.* **2020**, *142*, 7012; b) C. Wang, J. Liang, M. Jiang, X. Li, S. Mukherjee, K. Adair, M. Zheng, Y. Zhao, F. Zhao, S. Zhang, et al., *Nano Energy* **2020**, *76*, 105015; c) C. Yu, Y. Li, K. R. Adair, W. Li, K. Goubitz, Y. Zhao, M. J. Willans, M. A. Thijs, C. Wang, F. Zhao, et al., *Nano Energy* **2020**, *77*, 105097.
[16] M. Weiss, F. J. Simon, M. R. Busche, T. Nakamura, D. Schröder, F. H. Richter, J. Janek, *Electrochem. Energy Rev.* **2020**, *3*, 221.
[17] S. Wenzel, T. Leichtweiss, D. Krüger, J. Sann, J. Janek, *Solid State Ionics* **2015**, *278*, 98.
[18] S. Wenzel, S. Randau, T. Leichtweiß, D. A. Weber, J. Sann, W. G. Zeier, J. Janek, *Chem. Mater.* **2016**, *28*, 2400.
[19] S. Wenzel, D. A. Weber, T. Leichtweiss, M. R. Busche, J. Sann, J. Janek, *Solid State Ionics* **2016**, *286*, 24.
[20] S. Wenzel, S. J. Sedlmaier, C. Dietrich, W. G. Zeier, J. Janek, *Solid State Ionics* **2018**, *318*, 102.
[21] P. Hartmann, T. Leichtweiss, M. R. Busche, M. Schneider, M. Reich, J. Sann, P. Adelhelm, J. Janek, *J. Phys. Chem. C* **2013**, *117*, 21064.
[22] a) Z. Liu, A. Borodin, G. Li, X. Liu, Y. Li, F. Endres, *J. Phys. Chem. C* **2020**, *124*, 300; b) S. Boulineau, J.-M. Tarascon, J.-B. Leriche, V. Viallet, *Solid State Ionics* **2013**, *242*, 45; c) S. Wang, Y. Zhang, X. Zhang, T. Liu, Y.-H. Lin, Y. Shen, L. Li, C.-W. Nan, *ACS Appl. Mater. Interfaces* **2018**, *10*, 42279.
[23] G. J. Brug, A. van den Eeden, M. Sluyters-Rehbach, J. H. Sluyters, *J. Electroanal. Chem. Interfacial Electrochem.* **1984**, *176*, 275.
[24] S. Wenzel, T. Leichtweiss, D. A. Weber, J. Sann, W. G. Zeier, J. Janek, *ACS Appl. Mater. Interfaces* **2016**, *8*, 28216.
[25] X. Liang, Q. Pang, I. R. Kochetkov, M. S. Sempere, H. Huang, X. Sun, L. F. Nazar, *Nat. Energy* **2017**, *2*, 17119.
[26] A. L. Santhosha, L. Medenbach, J. R. Buchheim, P. Adelhelm, *Batteries Supercaps* **2019**, *2*, 524.

Manuscript received: November 15, 2020
Accepted manuscript online: December 14, 2020
Version of record online: February 1, 2021

  